Biochemical and Biophysical Research Communications **282,** 219–227 (2001)
doi:10.1006/bbrc.2001.4568, available online at http://www.idealibrary.com on IDEAL®

Toward the Three-Dimensional Structure of the *Escherichia coli* DNA-Binding Protein H-NS: A CD and Fluorescence Study

Oliver Schröder,[1] Detlev Tippner, and Rolf Wagner[2]
Institut für Physikalische Biologie, Heinrich-Heine-Universität Düsseldorf, Universitätsstrasse 1, D-40225 Düsseldorf, Germany

Received February 14, 2001

The DNA-binding protein H-NS compacts DNA and acts as a specific transcription factor regulating the expression of various bacterial genes. The small abundant protein binds to curved DNA without apparent sequence specificity and the exact nature of its DNA interaction is still unknown. H-NS lacks any common DNA-binding or oligomerization motif and except for a C-terminal fragment of the protein no high resolution structural information is available today. Since the complete structure of H-NS is of considerable interest for understanding its versatile regulatory features, and in lack of high-resolution data for the complete molecule, we have combined circular dichroism (CD) and fluorescence measurements to collect secondary- and higher-order structural information on H-NS. Comparison of CD analyses of wild type H-NS and functional defective mutants allowed assigning secondary structure elements to the N-terminal oligomerization domain of the protein. Moreover, according to fluorescence energy-transfer data we calculate a 45 Å distance between the DNA-binding and the oligomerization domain of H-NS.

Key Words: **H-NS; H-NS mutants; secondary structure; circular dichroism; fluorescence energy-transfer.**

The *Escherichia coli* protein H-NS is a small (136 amino acids, 15.6 kDa) abundant compound of the bacterial nucleoid which is of particular interest for its central role in modulating the expression of many environmentally regulated genes (1). It belongs to the family of bacterial DNA-binding proteins and is known to interact specifically with intrinsically curved DNA in a fairly sequence-independent manner (2, 3). The protein is highly conserved among enteric bacteria but from the primary sequence there is no convincing similarity to any other DNA-binding protein and no sequence motif characteristic for DNA binding is evident. Although specific H-NS/DNA complexes have been analyzed by footprinting and fluorescence studies which revealed two modes of DNA recognition, the exact nature of the H-NS/DNA interaction is still unknown. It is also not entirely clear whether H-NS binds to the small or large groove of helical DNA (4–6). H-NS has been shown to function as a global control element in bacterial gene expression acting on the levels of transcription as well as translation. While for many genes H-NS acts as transcriptional repressor for some genes it can also have activator function (7, 8). Due to its peculiar DNA binding properties the mechanism by which H-NS influences transcription is prone to be distinct from other typical transcription factors (9). The protein has been postulated to interact with the DNA in an oligomeric form since it has been shown to undergo self-association (6) which affects its DNA binding behavior and ability to induce DNA bending. The molecular mechanism of H-NS oligomerization is still undiscovered and various studies report that H-NS may exist as a dimer, tetramer or small oligomer in solution and may even aggregate to higher multimers, depending on the conditions and type of analysis (10–12). It is probably this tendency which has so far hampered a detailed structural analysis for the complete molecule. Only a 47-amino acid C-terminal fragment (position 90 to 136) has been studied by NMR spectroscopy. This fragment apparently encompasses the DNA-binding domain and consists of an antiparallel β-sheet, an α-helix and a 3_{10}-helix which form a hydrophobic core (13). Biochemical studies and studies with protein mutants indicate that the protein very likely has a modular structure with a DNA-binding domain located in the C-terminal half and an oligomerization and regulatory domain in the center and the

[1] Present address: Center for Molecular Genetics, University of California at San Diego, 9500 Gilman Drive, La Jolla, California 92093-0634.
[2] To whom correspondence should be addressed. Fax: 49 211 811 5167. E-mail: R.Wagner@mail.rz.uni-duesseldorf.de.

0006-291X/01 $35.00

N-terminal half of the protein (11, 12, 14). However, recent work has also suggested that mutations in the C-terminal region may affect the oligomeric state of the protein (6). Hence, except several secondary structure predictions a complete picture of the overall H-NS structure and its functional domains is still not at hand. In lack of any available high resolution structural information for the complete molecule we have attempted in this study to gain more complete secondary and higher order structural data by CD and fluorescence spectroscopic methods. Here, we perform CD measurements of H-NS and mutants thereof and assign specific secondary structural elements to the N-terminal half of the protein. Moreover, utilizing fluorescence energy-transfer techniques, we calculate a relatively high spacial distance between the two major functional domains consistent with the view that they exist as separate domains which may function independently within the context of the full-length protein.

MATERIALS AND METHODS

Protein purification. Wild type H-NS was purified from stationary MRE600 cells (15). The cells were disrupted by grinding with aluminum oxide (Alcoa) and the lysate was used to prepare a ribosome-free supernatant as described before (16). After high-speed centrifugation the supernatant was further purified by a fractionated ammonium sulphate precipitation (30–60%) followed by chromatography on P11 phosphocellulose (Whatman). Proteins were eluted with a linear salt gradient (0.05–1.5 M KCl) in PG-buffer (50 mM Na-phosphate, pH 7.4, 50 mM KCl, 10 mM β-mercaptoethanol, 10 mM EGTA, 10% glycerol, 23 μg/ml PMSF). Further purification was achieved after heparin sepharose 6B (Sigma) chromatography using a linear salt gradient (0.05–1.5 M KCl) in PG buffer. After pooling and concentrating the H-NS containing fractions using ultrafiltration tubes (Amicon), remaining contaminants were removed by a final FPLC gelfiltration step (TSK Biosep-SEC-S400, Phenomenex). The FPLC fractions were routinely tested for purity and specific DNA binding activity on SDS–PAGE and gel retardation assays using a specific *rrnB* P1 promoter fragment, respectively.

H-NS(R12C) was expressed from plasmid pHM12 transformed into the OmpT-deficient *E. coli* strain CU288 (both kindly provided by T. Mizuno, Nagoya University, Japan) after induction with 1 mM IPTG. After 15 h at 37°C cells were sedimented, then resuspended in extraction buffer (20 mM Tris–HCl, pH 7.5, 100 mM NH_4Cl, 10 mM Mg-acetate, 10 mM β-mercaptoethanol) and lysed in a french pressure cell. The subsequent H-NS(R12C) purification was done as described above, with the exception that all buffers contained additional protease inhibitors (1 μM pepstatin, 1 μM leupeptin, and 0.2 mM PMSF) and the pH during P11 chromatography was lowered to 6.5.

H-NS(R54C) was expressed from HM40 cells (CU241 *hns40* (R54C) *zch-506::*Tn*10;* kindly provided by T. Mizuno). Fifty to sixty grams of stationary cells were accumulated, then resuspended in extraction buffer and lysed in a french pressure cell. The subsequent H-NS(R54C) purification was carried out as described for the wild type protein, with the exception that all buffers contained additional protease inhibitors (1 μM pepstatin, 1 μM leupeptin and 0.2 mM PMSF, 4 mM benzamidine hydrochloride) and the pH during P11 chromatography was lowered to 6.5. In designation of the amino acid mutants we followed the published nomenclature (14). Note, however, that the actual sequence positions deviate by 1.

Circular dichroism spectroscopy. CD spectra of H-NS were measured using a Jasco J-715 spectropolarimeter calibrated with ammonium d-camphor-10-sulfonate. The CD measurements were carried out in a wavelength range between 185 and 260 nm in a cell with a path length of 0.1 cm (volume 200 μl) at 25°C unless otherwise stated. The spectra are the average of two or three independent measurements of each five scans recorded in 1 nm increments at a scan speed of 10 nm/min, 1 nm band width, 20 mdeg sensitivity, and a 1 s time constant. Prior to all measurements, proteins were extensively dialyzed against 10 mM Na-phosphate, pH 7.2, 1 mM DTT, and then analyzed at final concentrations between 60–140 μg/ml (4–9 μM).

For the temperature dependent measurements a thermostat-controlled waterbath (heating/cooling capacity 1.5°C/min) was connected to the cell and equilibration of the cell volume to the desired temperature was ensured by a 15 min incubation between each step before reading the spectra was resumed.

CD data analysis. Secondary structure composition of H-NS was analyzed from its CD spectra by two methods: (1) The Singular-Value-Decomposition (SVD), which determines the fraction of residues in α-helical, β-sheet, β-turn, and unordered conformations in the protein under investigation using CD data of proteins with known secondary structures. For that purpose, we utilized the DicroPlot V 2.4 software, which offers a Variable Selection variant of the SVD (17). (2) The CD Spectra Deconvolution (CDNN) method, which compares patterns in secondary structure elements of proteins with known structure and identifies correlations in the obtained CD data (18, 19).

Fluorescence studies. Fluorescence measurements were performed in an SLM 800 photon-counting spectrofluorometer with a xeneon arc lamp. All spectral measurements were carried out at 21°C. The excitation and emission slit width were 8 and 4 nm, respectively. The absorption of the sample was kept low to avoid inner-filter quenching.

Fluorescence labelling of H-NS. The thiol-specific fluorescence marker *N*-(1-pyrenyl)maleimide (Sigma) was used as fluorescence acceptor. It was coupled to the unique cysteine at position 20 of H-NS (Cys20) according to published procedures (20). The reaction was performed for 4 h at 4°C in the dark and the progress was monitored spectroscopically using the molar extinction coefficients for H-NS ($\epsilon_{278} = 0.89\ 1\ g^{-1}\ cm^{-1}$) and pyrene ($\epsilon_{340} = 2.2 \times 10^4\ M^{-1}\ cm^{-1}$). Excess reagent was quenched with a 10 fold molar excess of glutathione for 1 h at 4°C and H-NS was separated from reactants by micro dialysis. The efficiency of the coupling reaction was between 0.8 to 1.0 mol of pyrene per mol H-NS. The fluorescence labeled H-NS derivative is designated $H\text{-}NS_{PM}$.

Measurement of the distance between donor and acceptor by Förster's theory. The internal singular tryptophane of H-NS (Trp108) was used as fluorescence donor. According to Förster's theory (21), the dipole–dipole energy-transfer efficiency T between a donor and acceptor molecule is related to the distance r by

$$r = R_0((1/T) - 1)^{1/6} \quad [1]$$

or

$$T = r^{-6}/(r^{-6} + R_0^{-6}). \quad [2]$$

T can also be expressed as

$$T = 1 - (Q/Q_0) \quad [3]$$

with Q and Q_0 as quantum yields of donor in the presence and absence of acceptor, respectively.

R_0, representing the distance (angstroms) at which the transfer efficiency equals 50% is given by

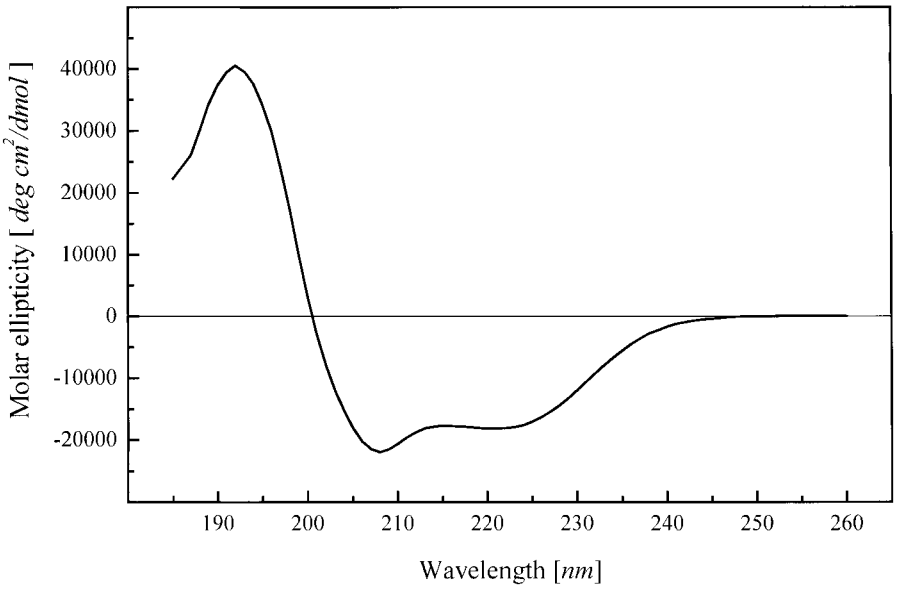

FIG. 1. CD spectrum of H-NS in 10 mM Na-phosphate, pH 7.2, 10 mM DTT at 25°C. The graph represents the mean of three independent measurements with protein concentrations between 4 and 9 μM. The spectrum has a maximum at 192 nm (molar ellipticity $\Theta = 40507$) and minima at 208 ($\Theta = -21960$) and 220 nm ($\Theta = -18137$; see also Table 1).

$$R_0 = 9.79 \times 10^3[(J)Q \cdot (n^{-4})(\kappa)^2]^{1/6}, \quad [4]$$

where n is the refractive index of the medium between donor and acceptor (taken as 1.4). $(\kappa)^2$ represents the orientation factor of both donor and acceptor which is taken as 2/3 (22, 23). J is the spectral overlap integral between the emission spectrum of the donor and the absorption spectrum of the acceptor. It is given by

$$J(\mathrm{M}^{-1}\,\mathrm{cm}^3) = \frac{\int F_d(\lambda)\epsilon_a(\lambda)\lambda^4 d\lambda}{\int F_d(\lambda) d\lambda}, \quad [5]$$

where $F_d(\lambda)$ and $\epsilon_a(\lambda)$ are the relative fluorescence intensity (%) of the donor and the molar extinction coefficient (M^{-1} cm^{-1}) of the acceptor, respectively. λ is the wavelength at nanometer interval, $d\lambda$.

The spectral overlap integral $J = 1.839\ 10^{-14}$ M^{-1} cm^3 was calculated according to [5]. The quantum yield, Q_S, of a sample was determined by comparison with a reference sample (photon counter) as described (24)

$$Q_S = \frac{Q_R(1 - 10^{A_R})(area)_S n_R^2}{(area)_R(1 - 10^{-A_S})n_S}, \quad [6]$$

where n is the refractive index of the solvent, A the absorption of the sample and *area* the integral of the respective fluorescence intensities between 300 and 400 nm. S and R refer to the sample and the reference, respectively. 1-anilino-8-naphthalene sulfonate (ANS) with known quantum yields in ethanol and methanol was used as reference (25) and the validity of the measurement was checked by comparison of the quantum yields.

RESULTS AND DISCUSSION

CD Spectrum of H-NS

Despite intensive effort structural data (i.e., from X-ray diffraction) on the H-NS protein is still incomplete, although NMR studies on several isolated C-terminal portions of H-NS have been conducted recently (13, 26). Thus, except several computational secondary structure predictions, e.g. (27), a thorough picture of the overall protein structure of H-NS remains elusive up to date. This is very unfortunate since the primary amino acid sequence of H-NS exhibits neither known oligomerization nor DNA binding motifs, both being important with regard to the unusual and interesting specificity of H-NS for AT-rich, curved DNA sequences and the ability to bend the bound DNA (28). Here, we perform CD spectroscopy of H-NS and mutants thereof with functional defects in order to explore the structural organization of H-NS and assign specific functions to its structural domains.

First, we assayed the CD spectroscopic properties of the wild type H-NS protein to obtain a reliable prediction on the overall structural composition of H-NS. For this purpose, we used 4–9 μM fractions of FPLC-purified protein to compose the CD spectrum from 185 to 260 nm according to the procedures described under Materials and Methods. Figure 1 shows the resulting CD spectrum of H-NS, exhibiting a strong maximum at 192 nm and two minima at 208 and 220 nm, respectively (see also Table 1). Since a strong positive band near 190 nm and two negative bands near 208 and 222 nm are considered to be characteristic for α-helical structures (29), the shape of the obtained spectrum clearly indicates a high content of α-helical structures within the H-NS protein. For a detailed calculation of the structural composition of H-NS, we took advantage of two different procedures to calculate the secondary

TABLE 1

Properties of the CD Spectra of H-NS, H-NS(R12C), and H-NS(R54C)

Protein	max/Θ	min I/Θ	min II/Θ	ip
H-NS	192/40507	208/−21960	220/−18137	200–201
H-NS (R12C)	192/40442	208/−22456	220/−18849	200–201
H-NSY (R54C)	193/25330	209/−13238	222/−11802	201–202

Note. The table summarizes the maxima (max) and minima (min I and min II) of the CD spectra and the respective molar ellipticities (Θ) at these wavelengths. The positions of the isodicroitic points (ip) are also indicated. Note that the precision of the values is limited by the increments (1 nm) at which the scans have been recorded.

structure content based on the obtained spectroscopic data. The first method is a Singular-Value-Decomposition (SVD) estimate using CD data of proteins with known secondary structures to calculate the fraction of residues in α-helical, β-sheet, β-turn, and unordered conformations in the protein under investigation. For this purpose the DicroPlot V 2.4 software was employed (17). The second method computes the structural content of a protein using the CD Spectra Deconvolution software (CDNN), which identifies patterns and correlations in the obtained CD data (18, 19).

Both approaches, though to a different extent, corroborate the interpretation inferred from the spectrum such that the H-NS protein predominantly consists of α-helical structures (47–57%), whereas only 8–14% contain β-sheets, 14–15% are turns and another 21–24% are random structures (Table 2, a and b). These numbers are also in good correspondence to recent CD measurements of an N-terminal part of H-NS purified from *Salmonella typhimurium* (11) and several secondary structure predictions, which augur the approximately first 65 N-terminal amino acids and a C-terminal region of the 136 amino acid protein to be predominantly of α-helical structure (data not shown).

CD Spectra of Mutant H-NS Proteins

Next we attempted to assign certain structural elements to specific functions. To this aim we examined possible changes of the overall structural composition of H-NS resulting from specific amino acid substitutions, which render the protein inactive. We focused on the less characterized N-terminal half of the protein and measured the CD spectra of the two mutant proteins H-NS(R12C) and H-NS(R54C). Both these mutations have been shown to affect the activity of H-NS as a transcriptional regulator, H-NS(R12C) being deficient in transcriptional repression and H-NS(R54C) failing in correct oligomerization (14). As shown in Fig. 2, H-NS(R12C) yields a CD spectrum that is almost identical to that of the wild type protein, demonstrating that no major changes in the overall protein structure occur when arginine 12 is substituted with a cysteine. However, the second H-NS mutant analyzed, H-NS(R54C), exhibits clearly different spectroscopic properties. Its bands peak with significantly lower magnitudes and are slightly shifted towards higher wavelengths (see also Table 1), indicating drastic changes in the structural composition (i.e., α-helical content) of H-NS due to the substitution of arginine 54 with a cysteine residue. The subsequent analysis of the obtained CD data confirms these observations such that the calculated distribution of secondary structures in H-NS(R12C) is almost identical to that of the wild type protein, while H-NS(R54C) contains significantly less α-helical residues (31–36% vs 47–57% in the wild type) and a higher amount of unordered, random structures (Table 2).

Taken together, these results imply that the analyzed amino acid substitution at residue 12 does not affect the structural integrity of H-NS, whereas the substitution at residue 54 impairs the ability to acquire the wild type structure by interfering with the formation of a α-helical element in the N-terminal domain of H-NS. This notion is supported by various secondary structure predictions which augur arginine 54 with high probabilities to be part of an α-helical structure (not shown). Since H-NS(R54C) has already been shown to be deficient in oligomerization (14), it is conceivable to assume that this α-helical element is integral to the protein–protein association of H-NS.

TABLE 2

CD Data Analysis to Determine the Secondary Structure Composition of H-NS, H-NS(R12C), and H-NS(R54C)

	Secondary structure content [%]				
Protein	α	pβ	aβ	t	rc
			a		
H-NS	46.7	10.0	4.7	14.7	24.0
H-NS (R12C)	47.4	9.2	6.2	13.0	23.6
H-NS (R54C)	31.5	14.5	4.5	19.0	30.0
			b		
H-NS	57.3	3.2	5.3	14.8	21.3
H-NS (R12C)	60.0	2.4	5.3	14.3	20.3
H-NS (R54C)	35.8	9.9	6.3	17.5	29.6

Note. The data were obtained from the spectra shown in Fig. 2. Indicated are the fractions of residues in α-helical (α), parallel β-sheet (pβ), antiparallel β-sheet (aβ), turn (t), and random coil (rc) conformation in percent for every investigated protein. (a) Results after calculation by Singular-Value-Decomposition (SVD) utilizing DicroPlot V 2.4 (17). (b) Summary of the CD Spectra Deconvolution (CDNN) end results. The table shows the averaged results of calculations at various wavelength ranges (190/195/200/210–260 nm) (18, 19).

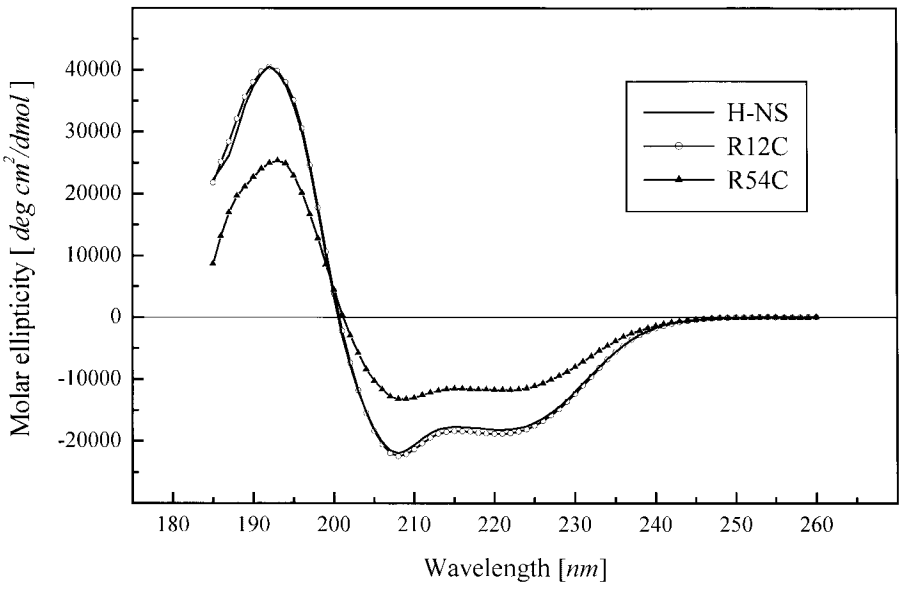

FIG. 2. CD spectra of H-NS, H-NS(R12C), and H-NS(R54C) in 10 mM Na-phosphate, pH 7.2, 10 mM DTT at 25°C. The graphs represent the mean of three independent measurements for each protein with protein concentrations between 4 and 9 μM. H-NS(R12C) exhibits CD spectroscopic properties almost identical to wild type H-NS with a maximum at 192 nm (Θ = 40442) and minima at 208 nm (Θ = −22456) and 220 nm (Θ = −18849), respectively. H-NS(R54C) displays significantly different characteristics with a maximum at 193 nm (Θ = 25330) and minima at 209 nm (Θ = −13238) and 222 nm (Θ = −11802), respectively (see also Table 1).

Temperature-Dependent CD Measurements

For a more detailed analysis on the structural effects of the amino acid mutations we performed temperature-dependent CD measurements. For that purpose, we monitored the CD spectra of wild type H-NS and the two mutant proteins during thermal denaturation and renaturation. A stepwise increase of the temperature from 24 to 64°C allowed us to follow the unfolding process of the three proteins, while the subsequent incremental decrease of the temperature monitored the refolding of the proteins.

As shown in Fig. 3a, partial thermal denaturation of wild type H-NS is accompanied by clear changes in the molar ellipticities at 192, 208, and 220 nm, indicating the unfolding of the structural components responsible for these bands. Additionally, this notable increase of unordered structures at 64°C is denoted by shifts in the maximum, minima and isodicroitic point. This is expected, since unordered structures characteristically yield strong negative bands near 200 nm and a much weaker (generally positive) band at higher wavelengths (29). Therefore, the striking decrease of the maximum at 192 nm and the increase of the molar ellipticities between 200–220 nm are consistent with a augmentation of unordered structures during thermal denaturation of H-NS. The spectra taken during renaturation (Fig. 3b) reveal that the observed denaturation is roughly reversible, however, the original properties of the protein are not entirely restored after the denaturing/renaturing process.

CD measurements have been widely used to follow the equilibrium between helical structures and unordered conformations. Proteins undergoing helix–coil transitions in response to changes in temperature, pH or ionic strength typically exhibit an isodicroitic point near 203 nm (30). In these cases, the molar ellipticity at 220 nm is commonly measured in order to monitor the transition of α-helical to unordered structures, since both helical and unordered conformations exhibit characteristic signals at this wavelength. Therefore, we analyzed the amplitude of the CD signal of wild type H-NS at 220 nm as a function of the temperature (Fig. 4). The sigmoidal shape of the resulting denaturation curve indicates a monophasic helix–coil transition of the protein within the analyzed temperature range, suggesting the absence of stable intermediates and allowing calculation of a regression and a T_m value for this transition (40.81°C).

Based on these data, the following experiment was conducted to relate the helix–coil transitions of the mutant proteins to the wild type protein. We measured the changes of the molar ellipticity at 220 nm within the same temperature range for the two protein mutants and compared them to the wild type protein. As shown in Fig. 5, the resulting denaturation curves for the mutant proteins H-NS(R12C) and H-NS(R54C) imply monophasic helix–coil transitions similar to wild type H-NS. However, H-NS(R54C) displays notable quantitative differences. Its denaturation curve is shifted to higher molar ellipticities and exhibits a

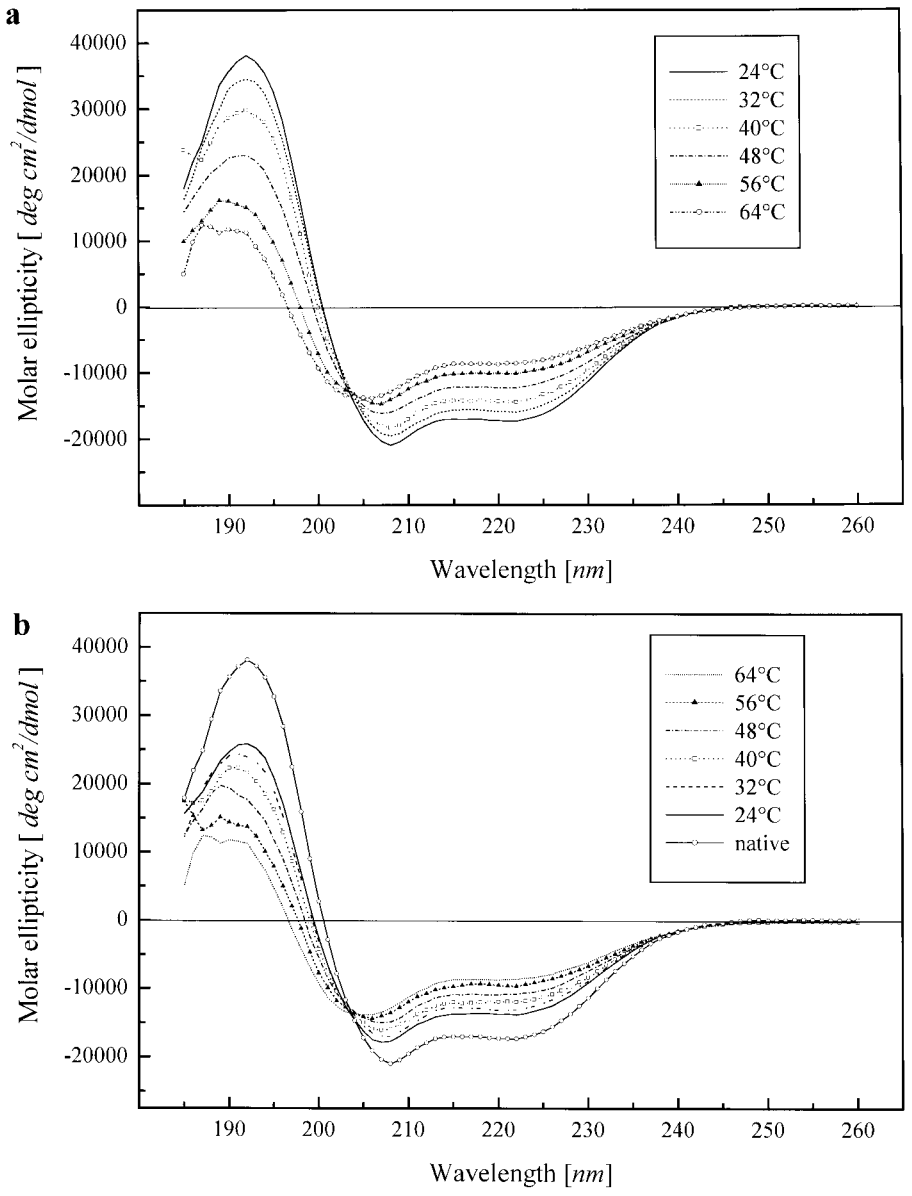

FIG. 3. Temperature-dependent CD measurements of H-NS. (a) Thermal denaturation of H-NS followed by CD spectroscopy. Starting at 24°C, the cell temperature was increased stepwise by increments of 8°C, ending at 64°C, and a CD spectrum was recorded at each temperature. The respective CD spectra are summarized in the graphics, the according temperatures are indicated in the upper right window. (b) Thermal renaturation of H-NS. Renaturing of the protein was monitored during a stepwise decrease of the temperature by 8°C increments, ending at 24°C. A spectrum was recorded at each temperature. The resulting CD spectra are summarized in the graphics, the according temperatures are indicated in the upper right window. The CD spectrum recorded at the beginning of temperature upshift/downshift series is indicated as "native."

much lesser slope and a higher T_m (47.30°C) compared to wild type H-NS. These data prove that the amino acid substitution at position 12 evidently does not alter the distribution of the structural elements (see above) and the helix–coil transition mode of H-NS, whereas the substitution of arginine 54 leads to a significantly different helix–coil transition behavior of the protein due to a variation in the structural composition (i.e., loss of α-helical elements). Together with the results shown above it is reasoning to conclude that the arginine substitution at position 54 impedes the formation of a stable α-helical structure and renders this region unordered within H-NS(R54C). The lesser slope of the helix–coil transition in this case can be explained by the fact that the stable helical structure, which transitions to an unordered form during thermal denaturation in the wild type protein and H-NS(R12C), is already randomly coiled in H-NS(R54C) due to the destabilizing effect of the arginine 54 substitution. This is confirmed by the data shown above affirming a

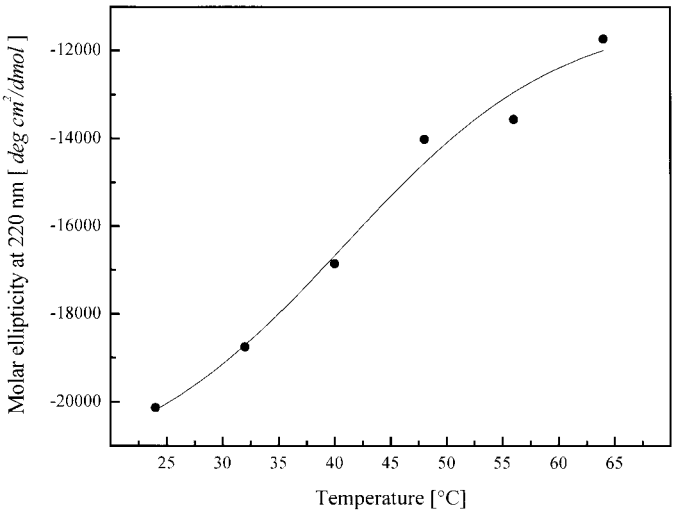

FIG. 4. Thermal denaturation curve of H-NS (helix–coil transition). The graph shows the amplitude at 220 nm of the CD signal of H-NS as a function of the temperature. The molar ellipticities at 220 nm were averaged from two independent measurements. The sigmoidal regression shows an upper asymptote at $\Theta = -11065$ and a lower asymptote at $\Theta = -21826$.

higher amount of unordered elements in this protein. Furthermore, the higher T_m of the helix–coil transition of H-NS(R54C) indicates that the structures involved are different from those assessed for the wild type protein and H-NS(R12C) at a lower T_m.

Altogether, these results are in good agreement with previous secondary structure predictions and CD data on the N-terminal half (residues 1–64) of H-NS (11), confirming that this segment contains helical structures with crucial functional importance. Cross-linking experiments with H-NS(1–64) indicate that this fragment encompasses a dimerization domain (31) and higher order self-association of the same protein fragment has been demonstrated to be coupled to the formation of a α-helical coiled–coil structure (11). H-NS(R54C) was furthermore originally isolated as a protein mutant with a severe defect in protein–protein association (14). The results presented in this study provide a structural explanation for the above observation. Hence, we deduce that the oligomerization of H-NS strongly depends on the formation of a α-helical element around arginine 54, which can be hampered by the amino acid substitution to a cysteine.

Proximity Relationship between N-Terminal and the C-Terminal Parts of H-NS

To collect additional information on the higher order proximity relationship between the N-terminal oligomerization domain and the C-terminal DNA-binding domain of H-NS we performed fluorescence measurements. For this purpose we utilized the intrinsic fluorescence of a single tryptophane residue at position 108 (Trp108) in the C-terminal part of the protein, which has previously been shown to be solvent exposed and linked to a protein conformational change when H-NS is bound to DNA (5). To determine the distance between this residue and the N-terminal dimerization part we took advantage of a single cysteine at position 20 (Cys20), which is accessible to sulfhydryl reagents and can thus readily be modified with a fluorescence label. We modified Cys20 with the thiol-specific reagent *N*-(1-pyrenyl)maleimide which can function as a fluorescence acceptor. This offers a convenient way to use fluorescence resonance energy transfer to estimate the distance between these characteristic positions within the H-NS molecule. These measurements revealed that the fluorescence emission spectrum of the donor (Trp108) has a substantial overlap with the pyrene absorption spectrum making both fluorescence molecules a very suitable donor/acceptor pair. The spectral overlap integral J has been calculated using equation [5] to be 1.839×10^{-14} (see Table 3). Values for the quantum yield Q, the energy-transfer efficiency T and the distance R_0 were calculated according to equations [1] to [6] and are summarized in Table 3. Based on these calculations a distance between the donor Trp108 and the acceptor Cys20 within H-NS_{PM} of 44.7 Å can be obtained.

A major source of uncertainty in fluorescence energy transfer measurements resides in the estimation of the orientation factor κ^2. When either the donor or acceptor are fixed within the structure values for κ^2 can vary

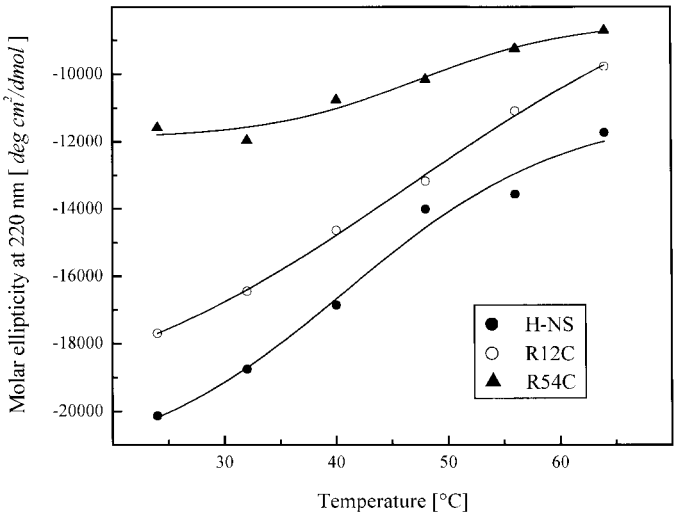

FIG. 5. Thermal denaturation curves of H-NS(R12C) and H-NS(R54C) in comparison to the wild type protein. The graphs show the amplitudes at 220 nm of the CD signals as a function of the temperature. The molar ellipticities were averaged from two independent measurements. The sigmoidal regression for H-NS(R12C) shows an upper asymptote at $\Theta = -6339$ and a lower asymptote at $\Theta = -20374$. The sigmoidal regression for H-NS(R54C) shows an upper asymptote at $\Theta = -8460$ and a lower asymptote at $\Theta = -11904$.

TABLE 3

Spectral Overlap, Quantum Yield, Energy-Transfer Efficiency, and Distance between Donor Trp108 and Acceptor $Cys20_{PM}$

Sample	Exitation wavelength (nm)	Emission wavelength (nm)	Spectral overlap integral, J (M^{-1} cm^3)	Quantum yield, Q	Distance at 50% energy-transfer efficiency, R_0 (Å)	Energy-transfer efficiency, T	Distance between donor and acceptor (Å)
H-NS	282	340	—	0.620	—	—	—
$H\text{-}NS_{PM}$	282	340	1.839×10^{-14}	0.509	34.7	0.179	44.7

between 0 and 4, depending on the respective orientation. If donor and acceptor are freely moving and isotropic in nature a value of 2/3 is generally used for κ^2 as in our case. Since both amino acid residues representing the donor and acceptor are solvent exposed we believe this assumption to be reasonable.

We can exclude that the distance measurement is affected in part by the formation of H-NS dimers (e.g., intermolecular distance) for the following reasons. First, we have analyzed H-NS for probable dimer formation by excimer fluorescence after modification of Cys20 with varying amounts the cysteine-specific reagent *N*-(1-pyrenyl)maleimide. Excimer fluorescence due to the formation of protein dimers should lead to a characteristic increase in fluorescence emission at 470 nm (20). No such increase could be observed giving a first indication that protein dimer formation might be inhibited. Second, Sephadex G100 gel chromatography revealed that the pyrenyl modified H-NS ($H\text{-}NS_{PM}$) in contrast to the unmodified protein only existed as monomer and not as dimer or higher multimers (data not shown). While this result demonstrates that the formation of $H\text{-}NS_{PM}$ dimers is severely impeded after modification of Cys20 within the N-terminal domain it also indicates that the results from the Förster's energy-transfer distance measurements exclusively reflect intramolecular fluorescence resonance energy transfer and not intermolecular transfer between donor and acceptor groups of an H-NS dimer pair.

A distance of about 45 Å between the C- and N-terminal domains of H-NS, as deduced from this study, appears to be rather large. It is consistent, however, with the probable dimensions of a 15 kDa protein and similar distances between separate domains are known for other small DNA binding proteins for which high resolution information is available (e.g., IHF or CRP). This distance supports the view of two structurally and functionally independent domains located at opposing protein surfaces. Our results therefore confirm earlier suggestions based on limited proteolysis studies and NMR measurements which proposed that the highly mobile C-terminal domain of H-NS is separated from the N-terminal half by a flexible amino acid linker (residues 82–90). According to these suggestions the C-terminal binding region forms an independent domain without inter-domain interactions (11, 32). The distance determined in this study is fully consistent with this view. However, the existence of independent domains is not supported by the report that mutations at position 115 (Pro115) can affect H-NS oligomerization (6). It is likely, therefore, that although structurally independent, the N- and C-terminal halves of H-NS both contribute to the observed cooperativity in DNA-binding. A likely mechanism for specific H-NS/DNA interaction could thus involve protein self-association coupled to the α-helical N-terminus *via* formation of coiled–coil structures and defined DNA-contacts through the C-terminal domain. Oligomerization may also represent the structural constraint for binding to curved DNA structures. In conclusion, our results corroborate a modular architecture of H-NS with clear structural separation between the dimerization and the DNA binding domains.

ACKNOWLEDGMENTS

We thank Reinhild Wurm for her skillfull help with the protein purification. We are indebted to C. Ueguchi and T. Mizuno for kindly providing us with the mutant H-NS expression systems. This work was supported by the Deutsche Forschungsgemeinschaft.

REFERENCES

1. Atlung, T., and Ingmer, H. (1997) H-NS: A modulator of environmentally regulated gene expression. *Mol. Microbiol.* **24,** 7–17.
2. Ussery, D. W., Hinton, J. C. D., Jordi, B. J. A. M., Granum, P. E., Seirafi, A., Stephen, R. J., Tupper, A. E., Berridge, G., Sidebotham, J. M., and Higgins, C. F. (1994) The chromatin-associated protein H-NS. *Biochimie* **76,** 968–980.
3. Williams, R. M., and Rimsky, S. (1997) Molecular aspects of the *E. coli* nucleoid protein, H-NS: A central controller of regulatory networks. *FEMS Microbiol. Lett.* **156,** 175–185.
4. Tippner, D., Afflerbach, H., Bradaczek, C., and Wagner, R. (1994) Evidence for a regulatory function of the histone-like *Escherichia coli* protein H-NS in ribosomal RNA synthesis. *Mol. Microbiol.* **11,** 589–604.
5. Tippner, D., and Wagner, R. (1995) Fluorescence analysis of the *Escherichia coli* transcription regulator H-NS reveals two distinguishable complexes dependent on binding to specific or non-specific DNA sites. *J. Biol. Chem.* **270,** 22243–22247.
6. Spurio, R., Falconi, M., Brandi, A., L., P. C., and O., G. C. (1997) The oligomeric structure of nucleoid protein H-NS is necessary for recognition of intrinsically curved DNA and for DNA bending. *EMBO J.* **16,** 1795–1805.
7. Ueguchi, C., Kakeda, M., and Mizuno, T. (1993) Autoregulatory

expression of the Escherichia coli *hns* gene encoding a nucleoid protein—H-NS functions as a repressor of its own transcription. *Mol. Gen. Genet.* **236,** 171–178.

8. Bertin, P., Terao, E., Lee, E. H., Lejeune, P., Colson, C., Danchin, A., and Collatz, E. (1994) The H-NS protein is involved in the biogenesis of flagella in *Escherichia coli. J. Bacteriol.* **176,** 5537–5540.
9. Schröder, O., and Wagner, R. (2000) The bacterial DNA-binding protein H-NS represses ribosomal RNA transcription by trapping RNA polymerase in the initiation complex. *J. Mol. Biol.* **298,** 737–748.
10. Ceschini, S., Lupidi, G., Coletta, M., Pon, C. L., Fioretti, E., and Angeletti, M. (2000) Multimeric self-assembly equilibria involving the histone-like protein H-NS. *J. Biol. Chem.* **275,** 729–734.
11. Smyth, C. P., Lundbäck, T., Renzoni, D., Siligardi, G., Beavil, R., Layton, M., Sidebotham, J. M., Hinton, J. C. D., Driscoll, P. C., Higgins, C. H., and Ladbury, J. E. (2000) Oligomerization of the chromatin-structuring protein H-NS. *Mol. Microbiol.* **36,** 962–972.
12. Ueguchi, C., Seto, C., Suzuki, T., and Mizuno, T. (1997) Clarification of the dimerization domain and its functional significance for the *Escherichia coli* nucleoid protein H-NS. *J. Mol. Biol.* **274,** 145–151.
13. Shindo, H., Iwaki, T., Ieda, R., Kurumizaka, H., Ueguchi, C., Mizuno, T., Morikawa, S., Nakamura, H., and Kuboniwa, H. (1995) Solution structure of the DNA binding domain of a nucleoid-associated protein, H-NS, from *Escherichia coli. FEBS Lett.* **360,** 125–131.
14. Ueguchi, C., Suzuki, T., Yoshida, T., Tanaka, K., and Mizuno, T. (1996) Systematic mutational analysis revealing the functional domain organization of *Escherichia coli* nucleoid protein H-NS. *J. Mol. Biol.* **263,** 149–162.
15. Cammack, K. A., and Wade, H. E. (1965) The sedimentation behaviour of ribonuclease-active and inactive ribosomes from bacteria. *Biochem. J.* **96,** 679–680.
16. Theissen, G., Thelen, L., and Wagner, R. (1993) Some base substitutions in the leader of an *Escherichia coli* ribosomal RNA operon affect the structure and function of ribosomes. *J. Mol. Biol.* **233,** 203–218.
17. Deléage, G., and Geourjon, C. (1993) An interactive graphic program for calculating the secondary structures content of proteins from circular dichroism spectrum. *Comp. Appl. Biosc.* **9,** 197–199.
18. Böhm, G., Muhr, R., and Jaenicke, R. (1992) Quantitative analysis of protein far UV circular dichroism spectra by neural networks. *Protein Eng.* **5,** 191–195.
19. Dalmas, B., Hunter, G., and Bannister, W. H. (1994) Prediction of protein secondary structure from circular dichroism spectra using artificial neural network techniques. *Biochem. Mol. Biol. Int.* **34,** 17–26.
20. Jung, K., Jung, H., and Kaback, K. (1994) Dynamics of lactose permease of *Escherichia coli* determined by site-directed fluorescence labeling. *Biochemistry* **33,** 3980–3985.
21. Förster, T. (1948) Zwischenmolekulare Energiewanderung und Fluoreszenz. *Ann. Phys.* **2,** 55–75.
22. Wu, P., and Brand, L. (1994) Resonance energy transfer: Methods and applications. *Anal. Biochem.* **218,** 1–13.
23. Kumar, K. P., Reddy, P. S., and Chatterji, D. (1992) Proximity relationship between the active site of *Escherichia coli* RNA polymerase and rifampicin binding domain: A resonance energy-transfer study. *Biochemistry* **31,** 7519–7526.
24. Parker, C. A., and Rees, W. T. (1960) Correction of fluorescence spectra and measurement of fluorescence quantum efficiency. *Analyst* **85,** 587–592.
25. Stryer, L. (1965) The interaction of a naphthalene dye with apomyoglobin and apohemoglobin. A fluorescent probe of nonpolar binding sites. *J. Mol. Biol.* **13,** 482–495.
26. Shindo, H., Ohnuki, A., Ginba, H., Katoh, E., Ueguchi, C., Mizuno, T., and Yamazaki, T. (1999) Identification of the DNA binding surface of H-NS protein from *Escherichia coli* by heteronuclear NMR spectroscopy. *FEBS Lett.* **455,** 63–69.
27. Falconi, M., Gualtieri, M. T., La Teana, A., Losso, M. A., and Pon, C. L. (1988) Proteins from the prokaryotic nucleoid: Primary and quaternary structure of the 15-kD *Escherichia coli* DNA binding protein H-NS. *Mol. Microbiol.* **2,** 323–329.
28. Afflerbach, H., Schröder, O., and Wagner, R. (1999) Conformational changes of the upstream DNA mediated by H-NS and FIS regulate *E. coli rrnB* P1 promoter activity. *J. Mol. Biol.* **286,** 339–353.
29. Woody, R. W. (1995) Circular dichroism. *Methods Enzymol.* **256,** 34–71.
30. Scholtz, J. M., and Baldwin, R. L. (1992) The mechanism of alpha-helix formation by peptides. *Ann. Rev. Biophys. Biomol. Struct.* **21,** 95–118.
31. Williams, R. M., Rimsky, S., and Buc, H. (1996) Probing the structure, function and interactions of the *Escherichia coli* H-NS and StpA proteins by using dominant negative derivatives. *J. Bacteriol.* **178,** 4335–4343.
32. Dorman, C. J., Hinton, J. C. D., and Free, A. (1999) Domain organization and oligomerization among H-NS-like nucleoid-associated proteins in bacteria. *Trends Microbiol.* **124,** 124–128.